Atmos. Chem. Phys. Discuss., 12, 22023–22057, 2012
www.atmos-chem-phys-discuss.net/12/22023/2012/
doi:10.5194/acpd-12-22023-2012

Atmospheric Chemistry and Physics Discussions

Diagnosing the transition layer in the extra-tropical lowermost stratosphere using MLS O_3 and MOPITT CO analyses

J. Barré[1], L. El Amraoui[1], P. Ricaud[1], J.-L. Attié[1,2], W. A. Lahoz[1,3], V.-H. Peuch[4], B. Josse[1], and V. Marécal[1]

[1]CNRM-GAME, Météo-France and CNRS URA1357, Toulouse, France
[2]Laboratoire d'Aérologie, Université de Toulouse, CNRS/INSU, Toulouse, France
[3]NILU, 2027 Kjeller, Norway
[4]ECMWF, Shinfield Park, Reading, UK

Received: 28 June 2012 – Accepted: 17 August 2012 – Published: 28 August 2012

Correspondence to: J. Barré (jerome.barre@meteo.fr)

Published by Copernicus Publications on behalf of the European Geosciences Union.

Abstract

The behavior of the Extra-tropical Transition Layer (ExTL) in the lowermost stratosphere is investigated using a Chemistry Transport Model (CTM) and analyses derived from assimilation of MLS (Microwave Limb Sounder) O_3 and MOPITT (Measurements Of Pollution In The Troposphere) CO data. We use O_3-CO correlations to quantify the effect of the assimilation on the height and depth of the ExTL. We firstly focus on a Stratosphere-Troposphere Exchange (STE) case study which occurred on 15 August 2007 over the British Isles (50° N, 10° W). We also extend the study at the global scale for the month of August 2007. For the STE case study, MOPITT CO analyses have the capability to sharpen the ExTL distribution whereas MLS O_3 analyses provide a tropospheric expansion of the ExTL distribution with its maximum close to the thermal tropopause. When MLS O_3 and MOPITT CO analyses are used together, the ExTL shows more realistic results and matches the thermal tropopause. At global scale, MOPITT CO analyses still show a sharper chemical transition between stratosphere and troposphere than the free model run. MLS O_3 analyses move the ExTL toward the troposphere and broaden it. When MLS O_3 analyses and MOPITT CO analyses are used together the ExTL matches the thermal tropopause poleward of 50°. This study shows that data assimilation can help overcome the shortcomings associated with a relatively coarse model resolution. The ExTL spread is larger in the Northern Hemisphere than the Southern Hemisphere suggesting that mixing processes are more active in the UTLS in the Northern Hemisphere than in the Southern Hemisphere. This work opens perspectives for studying the seasonal variations of the ExTL at extra-tropical latitudes.

1 Introduction

The Upper Troposphere/Lower Stratosphere (UTLS) plays a key role in chemistry-climate interactions. Carbon monoxide (CO) and ozone (O_3) concentrations change rapidly across the UTLS. High concentrations of O_3 (low concentrations of CO) in

ACPD
12, 22023–22057, 2012

the lower stratosphere contrast with low concentrations of O_3 (high concentrations of CO) in the upper troposphere. Holton et al. (1995) defined the lowermost stratosphere (LMS) as being below the 380-K isentrope and above the dynamical tropopause (usually defined between 1.5 and 3.5 Potential Vorticity Units, PVU, World Meteorological Organization, 1986). Previous studies, using in situ measurements of stratospheric and tropospheric trace gases, have shown that the LMS has intermediate characteristics between the troposphere and the stratosphere (Fischer et al., 2000; Hoor et al., 2002; Pan et al., 2004). Rapid changes in time and space of tracers at the UTLS are controlled by mixing processes between the stratosphere and the troposphere. An Extra-tropical Transition Layer (ExTL) of atmospheric tracers is present in the LMS above the extra-tropical dynamical tropopause.

Diagnostics using tracer-tracer correlation can locate the ExTL accurately. Fischer et al. (2000), Hoor et al. (2002) and Pan et al. (2004) used aircraft in-situ measurements to provide an analysis of trace gas (H_2O, CO, CO_2, N_2O, NO_y and O_3) correlations in the LMS. Trace gas correlations have been shown to be an effective method to diagnose stratosphere-troposphere exchange (STE) and mixing processes in the LMS region. Pan et al. (2007) proposed a set of three diagnostics to evaluate the representation of chemical transport processes in the extra-tropical tropopause. Hegglin et al. (2009) showed that these diagnostics can be applied to satellite measurements of O_3, CO and H_2O to characterize the ExTL seasonal and latitudinal variations in height and depth at the global scale. A multi-model assessment showed that models with coarse vertical resolution are unable to represent faithfully the ExTL at extra-tropical latitudes (Hegglin et al., 2010). Due to their coarse resolution, models overestimate the spread and the location in height of the ExTL.

To constrain the model used in this study, we assimilate O_3 stratospheric profiles from Aura/MLS (Microwave Limb Sounder) and Terra/MOPITT (Measurements Of Pollution In The Troposphere) CO tropospheric profiles into the MOCAGE (MOdèle de Chimie Atmospherique à Grande Echelle) chemical transport model (CTM). Data assimilation, which combines observational information and a priori information from a model

ACPD
12, 22023–22057, 2012

in an objective way (Kalnay, 2003), has the capability to reconcile different types of measurements such as nadir measurements (MOPITT CO) and limb measurements (MLS O_3). Data assimilation has also the capability to overcome possible deficiencies of the MOCAGE model in the UTLS region (see, e.g. Semane et al., 2007; El Amraoui et al., 2010; Barré et al., 2012). In this study, we propose to quantify the impact of the assimilation of O_3 and CO data on the extra-tropical tropopause region. We use the same case study as presented by El Amraoui et al. (2010) which considers a deep stratospheric intrusion on 15 August 2007 over the British Isles (50° N, 10° W). In this previous study, detailed validation demonstrated the capability of CO and O_3 analyses to better represent the STE. It was shown that CO analyses provide a better qualitative description of the event than O_3 analyses. The set of diagnostics proposed by Pan et al. (2007) are used for this STE event to quantify the capability of CO and O_3 analyses to represent the STE exchange for this case. We also propose to extend the set of diagnostics from regional to global scales in the extra-tropics for the month of August 2007. This allows us to quantify the capability of MOPITT CO and MLS O_3 assimilated fields to better estimate the chemical ExTL behavior in the tropopause region, from a single STE event at the regional scale to an average state of the atmosphere at the global scale. To our knowledge, this is the first time that these diagnostics have been used on chemical analyses from different types of satellite measurements (nadir and limb).

The paper is structured as follows. Section 2 provides the description of the model, the remote sensed data and the assimilation system. Section 3 provides a brief description of the STE event in August 2007 which was fully analyzed in El Amraoui et al. (2010). A set of diagnostics proposed by Pan et al. (2007) are used on this case study for the different assimilation experiments. Section 4 extends these diagnostics to the global scale in the extra-tropics in August 2007. Section 5 provides a discussion of results and conclusions.

ACPD
12, 22023–22057, 2012

2 Methodology

2.1 CTM and data assimilation system

The MOCAGE model is a three-dimensional CTM for the troposphere and the stratosphere (Peuch et al., 1999) which simulates the interactions between physical and chemical processes. It uses a semi-Lagrangian advection scheme (Josse et al., 2004) to transport the chemical species. It has 47 hybrid levels from the surface to ∼5 hPa with a resolution of about 150 m in the lower troposphere increasing to 800 m in the upper troposphere. Turbulent diffusion is calculated with the scheme of Louis (1979) and convective processes with the scheme of Bechtold et al. (2001). The chemical scheme used in this study is RACMOBUS. It is a combination of the stratospheric scheme REPROBUS (Reactive Procecesses Ruling the Ozone Budget in the Stratosphere, Lefèvre et al., 1994) and the tropospheric scheme RACM (Regional Atmospheric Chemistry Mechanism, Stockwell et al., 1997). It includes 119 individual species with 89 prognostic variables and 372 chemical reactions. MOCAGE has the flexibility to be used for stratospheric (El Amraoui et al., 2008a), tropospheric (Dufour et al., 2005) and UTLS studies (Ricaud et al., 2007; Barré et al., 2012). The meteorological analyses of Météo-France, ARPEGE (Courtier et al., 1991), are used to provide meteorological fields. In this study, the model has a global domain with an horizontal resolution of $2^\circ \times 2^\circ$.

The assimilation system used in this study is MOCAGE-PALM (Massart et al., 2005) implemented within the PALM framework (Buis et al., 2006). The technique used is 3D-FGAT (First Guess at Appropriate Time, Fisher and Andersson, 2001). This technique is a compromise between the 3D-Var (3-D-variational) and the 4D-Var (4-D-variational) methods. It compares the observations and the model background taking into account the measurement time and assumes that the increment to be added to the background state is constant over the entire assimilation window (in this case 3 h). The choice of this technique limits the size of the assimilation window, since it has to be short enough compared to chemistry and transport timescales. It has been validated

ACPD
12, 22023–22057, 2012

during the assimilation of ENVISAT data project (ASSET, Lahoz et al., 2007) and has produced good quality results compared to independent data and other assimilation systems (Geer et al., 2006). MOCAGE-PALM has been used to assess the quality of satellite O_3 measurements (Massart et al., 2007). The MOCAGE-PALM, assimilation products have been used in many atmospheric studies in relation to the O_3 loss in the Arctic vortex (El Amraoui et al., 2008a), tropics-mid-latitudes exchange (Bencherif et al., 2007), STE (Semane et al., 2007), exchange between the polar vortex and the mid-latitudes (El Amraoui et al., 2008b), and diagnosing STE from O_3 and CO fields (El Amraoui et al., 2010).

2.2 Aura/MLS O_3 and Terra/MOPITT CO observations

The MLS instrument onboard Aura uses limb sounding to measure chemical constituents (such as O_3) and dynamical tracers between the upper troposphere and the lower mesosphere (Waters et al., 2006). It provides global coverage with about 3500 profiles per day between 82° N and 82° S. In this study, we use Version 2.2 of the MLS O_3 dataset. This version provides profiles with about 3–5 km vertical resolution between 215 and 0.46 hPa. The along-track resolution of O_3 is ∼ 200 km between 215 and 10 hPa. The MLS data are selected following quality flags recommended in the MLS description document (see http://mls.jpl.nasa.gov/data/v2-2_data_quality_document.pdf). Measurements above 10 hPa are not used because of the upper limit of the MOCAGE model, 5 hPa. The measurement precision is in 0.04 ppmv (parts per million by volume) for lower altitudes (215 hPa) and of 0.2 ppmv for higher altitudes (10 hPa).

The MOPITT instrument (Drummond and Mand, 1996) is onboard the Terra platform and measures tropospheric CO with nadir-sounding. The horizontal resolution of MOPITT CO data (Version 3) is 22 km × 22 km. To prepare the MOPITT data for assimilation, super-observations are done by averaging data in latitude-longitude bins of 2° × 2°. The super-observations give around 8000 daily vertical profiles which are retrieved on 7 pressure levels (surface, 850, 700, 500, 350, 250 and 150 hPa). Information on the vertical sensitivity is provided by the averaging kernels, which are taken into account in

ACPD
12, 22023–22057, 2012

the assimilation system. At 500 hPa, the retrieval uncertainties are approximately 20 % in the tropics and at mid-latitudes, and 30–40 % at high latitudes.

2.3 Assimilation experiments

In this study, we use the same assimilation experiments performed by El Amraoui et al. (2010), hereafter LEA2010. The assimilation of MLS O_3 stratospheric and UTLS profiles and the assimilation of MOPITT CO tropospheric profiles started on 20 July 2007 and involve two independent runs (i.e. the assimilation experiments of O_3 and CO are done separately). The initial conditions for the assimilation were obtained by a free-model run started from the April climatological field. The assimilated fields of O_3 and CO have been validated for the month of July and August 2007 by LEA2010 using measurements from ozone sondes, aircraft and other remote sensing instruments. This validation exercise showed a better agreement of the analyses of each chemical species than the free-model runs. This previous study has also shown, in a qualitative manner, the added value of data assimilation on a STE case study on 15 August 2007. In the present study, we firstly propose to apply the diagnostics suggested by Pan et al. (2007) on the O_3-CO relationship in order to quantify the contribution of each assimilated species to the mixing processes in the UTLS. Secondly, we apply these diagnostics at the global scale in the extra-tropics for the month of August 2007.

3 STE case study on 15 August 2007

In this section, we present the case study of a STE event on 15 August 2007 over the British Isles. Figure 1 shows the O_3 and CO fields for MOCAGE and MOCAGE-PALM (MLS O_3 analyses and MOPITT CO analyses) in the tropopause region (260 hPa) between 35° N–75° N and 35° W–25° E. Figure 2 shows longitude-pressure cross sections at 59° N between 35° W and 25° E. These figures display the free model run CO fields (hereafter model CO) and MOPITT CO analyses (hereafter CO analyses) and free

ACPD
12, 22023–22057, 2012

model run O_3 fields (hereafter model O_3) and MLS O_3 analyses (hereafter O_3 analyses). The 380-K isentrope (black solid line) and the 2-PVU (white solid line) contours define the LMS height range. The STE event shows a deep stratospheric intrusion with high O_3 values (low CO values) coming from polar latitudes spreading southward over Western Europe.

In the latitude-longitude maps, O_3 analyses (Fig. 1c) show increased values in the STE structure compared to the model. Conversely, CO analyses (Fig. 1d) tend to exhibit decreased values in the STE structure compared to the model and also increased values around the STE. Along the vertical, O_3 analyses (Fig. 2c) show increased O_3 in the 200–300 hPa layer compared to the model O_3 field. LEA2010 showed that the O_3 maximum of 500 ppbv located in the intrusion (between 10° W and 0° W) shows a better agreement with independent data (MOZAIC flights and WOUDC ozone sondes) than the model O_3 run. For CO analyses, a minimum of CO in the cross section (Fig. 2d) is well reproduced within the stratospheric intrusion (between 10° W and 0° W) down to 400 hPa. At the LMS height range and at longitudes around the intrusion, the CO assimilated fields also display higher values than the model CO fields. LEA2010 also showed that CO analyses are in better agreement with independent data than the model CO run. LEA2010 suggested that O_3 analyses have the capability to better represent downward motions because higher O_3 values are entrained in the LMS and in the troposphere. LEA2010 also suggested that CO analyses have the capability to better represent upward (downward) motions, as higher (lower) CO values are represented in the UTLS than the model CO. A perspective of LEA2010 was to focus on the quantification of the contribution of O_3 and CO assimilated species in the mixing process between the stratosphere and the troposphere. To quantify the contribution of each experiment presented here, we have used the three diagnostics discussed by Pan et al. (2007):

1. O_3-CO correlations: to empirically select the CO and O_3 values which belong to the stratosphere, the troposphere and the ExTL.

ACPD
12, 22023–22057, 2012

2. Profile comparisons using relative altitude coordinates: to remove the geophysical variability from the planetary wave activity and to diagnose the effect of data assimilation on the UTLS CO and O_3 gradients.

3. Sharpness of the transition: to quantify the depth and the location of the ExTL.

3.1 Diagnostic 1: O_3-CO correlations

Tracer-tracer correlation methods help to identify the chemical transition between the stratosphere and the troposphere and the mixing processes in the LMS region (Fischer et al., 2000; Zahn et al., 2000; Hoor et al., 2002, 2004; Pan et al., 2004, 2007). In this section, we use O_3-CO correlations to determine empirically the chemical transition region from model and analysed fields. Figure 3 shows the O_3-CO relationships for model O_3 vs. model CO (Fig. 3a), O_3 analyses vs. model CO (Fig. 3b), model O_3 vs. CO analyses (Fig. 3c) and O_3 analyses vs. CO analyses (Fig. 3d). As described by Pan et al. (2007), the O_3-CO relationship is "L" shaped and has a stratospheric branch (high O_3 values and low CO values) and a tropospheric branch (low O_3 values and high CO values). These two branches can be represented by an approximate quasi-linear relation between O_3 and CO. Between these two branches the relationship between O_3 and CO is nonlinear due to the different chemical composition of the stratosphere and the troposphere.

We have applied the O_3-CO correlation diagnostic on 15 August 2007 12:00 UT between 30° W–10° E, 40° N–65° N where the STE takes place. The stratospheric branch, where high O_3 variability and low CO variability are observed, is empirically identified with a selection criterion defined by Pan et al. (2007). In Fig. 2, low CO values are mainly located in the stratosphere (above the 380-K isentrope) in the MOCAGE CO and in the MOPITT CO analyses. A quadratic fit is done with the CO values less than 25 ppbv. CO values which are below $+3\sigma$ (where σ is the standard deviation of the selected data) from the fit are considered as stratospheric (blue dots on Fig. 3). The tropospheric branch, where low O_3 variability and high CO variability are observed,

ACPD
12, 22023–22057, 2012

is also empirically identified with a selection criterion defined by Pan et al. (2007). In Fig. 2, these low O_3 values are mainly located in the troposphere (below the 2-PVU line) in the MOCAGE O_3 and in the MLS O_3 analyses. A linear fit is done with O_3 values lower than 70 ppbv. O_3 values which are lower than $+3\sigma$ from the fit are considered as tropospheric (red dots on Fig. 3). Between these two branches a set of points (green dots on Fig. 3) mark a transitional region which represents the ExTL between the stratosphere and the troposphere.

The "L" shape is detected in the four O_3-CO correlations but the transition region differs significantly between them. The transition region is composed by mixing lines corresponding to O_3-CO vertical relationships for each latitude-longitude location of the model. To illustrate this concept we have plotted in black the points located between 20° W and 0° W on the 59° N vertical plane corresponding to the stratospheric air mass intrusion displayed in the cross sections (Fig. 2). We also have over-plotted a quadratic fit of these points in Fig. 3; coefficients of the fit are provided in Table 1. The model O_3 vs. model CO shows a "convex" and compact relationship in the ExTL. This compact relationship shows that the mixing lines connecting the stratosphere and the troposphere at different locations are similar. Thus, the spatial variability of model CO and model O_3 fields is low in the ExTL. Compared to the model O_3 vs. model CO correlations, the O_3 analyses vs. model CO correlations show an increase of O_3 values in the ExTL. The relationship between O_3 analyses and model CO is less compact, showing different shapes of mixing lines at different locations illustrating the O_3 variability induced by MLS assimilation in the tropopause region (see Fig. 2c).

In the location of the intrusion, the mixing lines show a strong "concave" shape owing to the ozone maximum observed between 200 and 250 hPa and between 20° W and 0° W. Figure 3b shows that the O_3 analyses tended to increase in the ExTL region. The model O_3 vs. CO analyses correlations show a more angular "L" shape and a less compact relationship than model O_3 vs. model CO correlations. In this case CO values are decreased in the ExTL and tend to be increased in the upper troposphere (see Fig. 2d). This effect is seen in the location of the intrusion since the slope of the fit is

ACPD
12, 22023–22057, 2012

J. Barre et al.

decreased compared to the model O_3 vs. model CO fit. The minimum of CO visible in the analyses between 300 and 400 hPa and between 20° W and 0° W (Fig. 2d) (where the dynamical tropopause is the lowest in height) does not provide a significant change in the ExTL O_3-CO correlations. The O_3 analyses vs. CO analyses correlations show both the effect of MLS O_3 analyses and MOPITT CO analyses. In the ExTL, O_3 values are increased whereas CO values are decreased. The spread of the O_3-CO correlations in the ExTL is increased compared to the other O_3-CO correlations, showing an increased spatial variability of the O_3-CO mixing lines. In this section, we use O_3-CO correlations to select empirically the ExTL points. The impact of assimilation of O_3 and CO fields on the correlations is discussed. We also diagnose in the next sections, how the assimilation of MOPITT CO and MLS O_3 data affects the spatial extent of the ExTL.

3.2 Diagnostic 2: profile comparisons using relative altitude coordinates

In the second diagnostic, we analyze the tracer behavior in altitude coordinates relative to a chosen tropopause level. Because rapid changes in height of tracer concentrations happen near the tropopause, it is helpful to use a tropopause relative vertical coordinate to reduce the geophysical variability caused by wave activity at synoptic and planetary scales. The thermal tropopause has been used as a reference level by Pan et al. (2007, 2004) to calculate relative altitudes. The thermal tropopause defined by World Meteorological Organization (1957) and the dynamical tropopause defined by potential vorticity can provide double thermal or dynamical tropopause features related to Rossby wave breaking processes and associated transport (Pan et al., 2009; Homeyer et al., 2010). These double tropopause structures lead to difficulties in calculating diagnostics and in their interpretation. Figure 2 displays the location of the lower values of the thermal tropopause (green circles) and the 360-K isentrope level (green triangles). By taking into account O_3 and CO fields, the 360-K contour follows chemical variability in the UTLS. For these reasons, we have chosen to use the 360-K level as a reference level to calculate relative altitudes in order to reduce the geophysical variability in the CO and O_3 profiles. We do not assume that the 360-K level is the tropopause level.

ACPD
12, 22023–22057, 2012

Figure 4 provides O_3 and CO profiles in relative altitude (RALT) coordinates for the four O_3-CO correlations. Blue, red and green dots represent the stratospheric, the tropospheric and the ExTL CO and O_3 values, respectively, as selected in Sect. 3.1. Compared to the free model run, O_3 analyses (Fig. 4c) show more O_3 in the ExTL (green dots) and in tropospheric (red dots) regions. In relative altitude, the ExTL in the O_3 analyses extends into the troposphere by −6 km. It has been shown that the tropospheric O_3 concentrations in MLS analyses (with MOCAGE) are increased due to downward transport during the STE event (Barré et al., 2012). Thus, some increased upper tropospheric O_3 values are greater than the tropospheric threshold defined in Sect. 3.1. In the CO profiles, analyses (Fig. 4d) show CO values greater than the values of the free run in the tropospheric region and lower than the values of the free run in the stratospheric region. This leads to a stronger gradient in the ExTL around RALT = 0 km. Because of the selection criteria defined in Sect. 3.1, a stronger gradient gives a sharper extent of the ExTL in RALT coordinates. The distribution of the ExTL points differs significantly in the RALT space whether O_3 analyses and CO analyses are used separately or together. If we analyze the differences between Fig. 4c and Fig. 4e and between Fig. 4d and Fig. 4f, the selection of the ExTL points differs significantly. In the O_3 profiles, the upper bound of the ExTL (green dots) is decreased by about 1 km. In the CO profiles, the lower bound of the ExTL is decreased by about 2 km. CO analyses tend to sharpen in height the ExTL toward the lower stratosphere whereas O_3 analyses expand the ExTL toward the upper troposphere. Where CO analyses and O_3 analyses are used together, the ExTL is lowered by about 1 to 2 km. In the next section, we examine further the ExTL distribution in RALT space.

3.3 Diagnostic 3: sharpness of the transition

The third diagnostic provides the distribution of the ExTL in relative altitude space (as defined in Sects. 3.1 and 3.2). The shape of the ExTL distribution will allow us to quantify its location and depth. Figure 5a–d displays the distributions for the various O_3-CO relationships: model O_3 vs. model CO, O_3 analyses vs. model CO, model O_3 vs. CO

ACPD
12, 22023–22057, 2012

analyses and O_3 analyses vs. CO analyses, respectively. The vertical dashed red line and dotted red lines give the mean location of the thermal tropopause and the standard deviation from the mean, respectively. Table 2 provides the heights of the mean, the median and the standard deviation of the ExTL distributions in relative altitude space. The free model run distribution has its mean and median heights at about +0.5 km (1.5 km above the thermal tropopause) with a standard deviation of 1.4 km. This shows that the free model run has its ExTL following the 360-K surface in this case study. However, studies using in situ aircraft measurement show that the ExTL is centered on the thermal tropopause with a narrower extent than observed in this study (Pan et al., 2004, 2007). In a multi-model assessment, Hegglin et al. (2010) showed that models simulate a ExTL that is wider than observed in satellite observations, and shifted above the thermal tropopause. The low vertical resolution (800 m) in the model UTLS layers and also the low horizontal resolution ($2^\circ \times 2^\circ$) used in this study is not sufficient to represent the sharp gradients of O_3 and CO observed at the tropopause. This results in a broad transition region in the UTLS. Thus, in our case, a narrower and a lower altitude distribution would be considered an improvement.

Compared to the model O_3 vs. model CO distribution, the O_3 analyses vs. model CO distribution shows more spread with a standard deviation of 2 km (Fig. 5b and Table 2). The distribution is also skewed toward negative RALT coordinates. Pan et al. (2004) showed that skewed distributions, particularly toward negative relative altitudes, indicate active mixing from the stratosphere to the troposphere. The mean and the median values of the distribution are both about −0.4 km and the maximum of the distribution at −1.5 km is close to the thermal tropopause. As described in Sect. 3.2, an increase of tropospheric O_3 values leads to a broadering of the ExTL (down to RALT = −6 km) in the troposphere. No significant changes in the stratospheric region (positive RALT values) of the distribution can be noted. The increase of O_3 in the upper troposphere leads to increase the ExTL depth toward negative RALT. Due to the low sensitivity of the stratospheric selection criterion to the O_3 variations, the stratospheric region of the ExTL is not significantly modified. However, the STE is detected by the

ACPD
12, 22023–22057, 2012

tropospheric selection criterion. The ExTL distribution shows a maximum and a mean height corresponding to the thermal tropopause. This is consistent with Fig. 2c where the ozone gradient in the O_3 analyses follows the thermal tropopause.

Compared to model O_3 vs. model CO distribution and the O_3 analyses vs. model CO distribution, the model O_3 vs. CO analyses provides a narrower ExTL (Fig. 5c). The mean and the median of the distribution are very close to 0 km and the standard deviation is reduced to 1.1 km. Compared to the free model run, CO analyses increase the CO gradient between the stratosphere and the troposphere and show a narrower ExTL distribution. However, in this case study the STE characterized by low CO values in the upper troposphere is not detected by the tropospheric selection criterion (described in Sect. 3.1) which is not very sensitive to CO variations. Moreover, the stratospheric selection criterion is highly sensitive to CO variations. Compared to the model O_3 vs. model CO, the spread of the model O_3 vs. CO analyses distribution is reduced in the stratospheric region (positive RALT) whereas the tropospheric region (negative RALT) is not significantly modified. This lowers the mean value of the distribution.

The O_3 analyses vs. CO analyses distribution (Fig. 5d) has the same shape as the O_3 analyses vs. model CO distribution but is narrower. The maximum of the distribution (−1.5 km) is close to the thermal tropopause and the standard deviation (1.43 km) is lower than the standard deviation of the O_3 analyses vs. model CO distribution. The mean value of the O_3 analyses vs. model CO analyses distribution (−0.85 km) is close to the mean value of the thermal tropopause (−0.92 km). The ExTL distribution benefits from the combination of the information provided by O_3 analyses and CO analyses. The distribution is centered on the thermal tropopause with an extent narrower than the O_3 analyses vs. model CO distribution. Pan et al. (2004) found using aircraft measurements that the center of the ExTL is statistically associated with the thermal tropopause and the thickness of this layer is ∼2–3 km in the middle latitudes. The results found with the analyses are consistent with these previous studies (e.g. Hegglin et al., 2010). In Table 2, the thickness of the ExTL is ∼2.8 km (2σ) and the mean and median values are lowered by ∼1.4 km. Assimilation of data with vertical information

ACPD
12, 22023–22057, 2012

such as MLS stratospheric O_3 profiles or MOPITT CO profiles is well suited for improving the modeled ExTL in the UTLS. Moreover, because of the rapid overturning of air masses in the troposphere and high static stability in the stratosphere, stratosphere to troposphere transport (STT) shows deeper signatures in altitude than troposphere to stratosphere transport (TST) (Hoor et al., 2002). Consequently, during STT events, the ExTL will show a skewed distribution toward negative RALT. This skewed distribution is only seen with O_3 analyses which provide increased O_3 values in the LMS and below (see for example Fig. 2c) and allow detection of the appropriate STT in these diagnoses.

4 Global ExTL for the month of August 2007

In this section, we apply the diagnostic of Sect. 3.3 (Sharpness of the transition) in the extra-tropics for the month of August 2007 to investigate the impact of data assimilation of MOPITT CO and MLS O_3 on the ExTL representation at the global scale. The diagnostics have been performed on monthly-averaged model output. In this study, we only consider extra-tropical latitudes outside the 20° S–20° N range. Figure 6a–d shows zonal means of the model O_3, model CO, O_3 analyses and CO analyses for the month of August 2009, respectively. Black lines denote the LMS bounds (the lower black line is the 2-PVU level and the upper black line is the 380-K isentrope) and black dots give the thermal tropopause location in height. In general, O_3 analyses increase the amount of O_3 in the LMS, especially at northern extratropical latitudes poleward of 50° N (by more than 200 ppbv). CO analyses increase the tropospheric CO values, except between 20° N and 40° N, and decrease the lower stratospheric CO values.

We calculate the distribution of the O_3-CO ExTL for latitude bands of 10° between 90° S and 20° S and between 20° N and 90° N with the same selection criteria as in Sect. 3.1. To be consistent with Sect. 3, we choose to keep the 360-K level as a reference altitude for the RALT calculations. In Fig. 7, we provide the latitudinal variations of the ExTL distribution: median (red line), deciles (red to pink filled areas), mean (green

ACPD
12, 22023–22057, 2012

line) and standard deviation from the mean (light green lines) in RALT coordinates. The LMS bounds (the lower blue line is the 2-PVU level and the upper blue line is the 380-K isentrope) and the thermal tropopause (black dots) are also over-plotted in RALT coordinates. The ExTL distribution is provided for the four experiments: model O_3 vs. model CO, O_3 analyses vs. model CO, model O_3 vs. CO analyses and O_3 analyses vs. CO analyses. Table 3 provides mean, median and standard deviation values for the four regions marked by the dashed vertical lines on Fig. 6 (90° S to 50° S, 50° S to 20° S, 20° N to 50° N and 50° N to 90° N).

In the model O_3 vs. model CO distributions, the ExTL has latitudinal variations in the RALT space (Fig. 7a). In the Southern Hemisphere, the ExTL follows the 2-PVU line (mean and median values) although 0.5 to 1 km above it. Equatorward of 50° S the mean and median values are located between +0.5 km (20° N) and −1.5 km (50° N). Poleward of 50° S, the ExTL location in RALT decreases in height and matches the thermal tropopause (mean and median values −2.2 km). In the Northern Hemisphere, the ExTL is about +1.5 km at 20° N and +0.5 km 50° N. At higher latitudes, poleward of 50° N, the ExTL decreases to 0 km. This is about 2 km above the thermal tropopause. In both hemispheres, the standard deviations are reduced from tropical to polar latitudes by about 0.7 km. The standard deviation of the ExTL distribution shows higher values in the Northern Hemisphere. A wider extent of the ExTL corresponds to deeper exchanges between the stratosphere and the troposphere (see Sect. 3) and can be interpreted at the global scale as the STE activity strength. The wider extent of the ExTL in the Northern Hemisphere also suggests more intense mixing activity in summer than in winter. Two maxima of ExTL thickness are also identified in both hemispheres near 35° S and 35° N corresponding to the location of the subtropical jets where mixing processes occur (Gettelman et al., 2011). Pan et al. (2004) deduced from aircraft observations (in the Northern Hemisphere) of O_3 and CO a ExTL centered at the thermal tropopause with a thickness between 2 and 3 km expanding into a thicker layer in the vicinity of the subtropical jet.

ACPD
12, 22023–22057, 2012

The O_3 analyses vs. model CO data provides slightly wider distributions for the ExTL for all latitudes (Fig. 7b) with a standard deviation that is increased between +0.11 km and +0.29 km. When O_3 stratospheric profiles are assimilated, the model is unable to improve the strong O_3 gradients observed in the tropopause region. O_3 analyses move the ExTL location to lower altitudes and always have median and mean values of the distribution below the 380-K level in the LMS region. The mean values of the distributions are significantly lowered in the Northern Hemisphere by −0.42 km in the subtropics and by −0.74 km in the middle and polar latitudes closer to the thermal tropopause. This is due to an increase of ozone in the LMS especially in the Northern Hemisphere (Fig. 6c). Model O_3 vs. CO analyses (Fig. 7c) show reduction in the ExTL thickness. The layer thickness is strongly reduced as reflected in a reduction of the standard deviation by about −0.55 km in the Northern Hemisphere and by −0.2 km in the Southern Hemisphere. The mean and the median values match the thermal tropopause poleward of 50° S but remain 1 to 1.5 km above poleward of 50° N. The distribution of O_3 analyses vs. CO analyses has the best ExTL representation (Fig. 7d). The standard deviations are reduced, between −0.51 km and −0.22 km in the Northern Hemisphere. The mean and median values are consistent with the thermal tropopause location poleward of 50° S and 50° N. In the subtropical latitudes, the ExTL is located 2 km below the thermal tropopause. This region is subject to the thermal tropopause break at the location of the subtropical jet providing an instance of a double tropopause. By averaging the model outputs over one month, the double tropopause structures have been smoothed. It has been shown that the ExTL in this region has a contribution from the subtropical jet, the tropical tropopause layer and the mid-latitudes lowermost stratosphere, forming complex structures in the ExTL as double thermal tropopause features (Vogel et al., 2011). The examination of the subtropical ExTL merits further investigation but this is out of the scope of this paper.

As described in Sect. 3.1, stratospheric points are selected using a fit of CO values under 25 ppbv, and tropospheric points are selected using a fit of O_3 values under 70 ppbv. The stratospheric branch has low variability in CO and high variability in O_3.

ACPD
12, 22023–22057, 2012

The tropospheric branch has high variability in CO and low variability in O_3. During the MOPITT CO assimilation process, points in O_3-CO tracer space are only moved in the CO dimension quasi-tangentially to the tropospheric branch and quasi-perpendicularly to the stratospheric branch (see Fig. 3). During the MLS O_3 assimilation process, points in the O_3-CO tracer space are only moved in the O_3 dimension quasi-tangentially to the stratospheric branch and quasi-perpendicularly to the tropospheric branch. The upper bound of the ExTL distribution is mostly sensitive to CO variations whereas the lower bound of the ExTL distribution is mostly sensitive to O_3 variations. CO analyses have more influence on the stratospheric region of the ExTL and reduce the mixing layer depth. O_3 analyses have more influence on the tropospheric region of the ExTL and are not able to reduce the ExTL depth but have the capability to represent STE at extra-tropical latitudes.

In this section, we have shown that data assimilation helps to improve the ExTL representation between the stratosphere and the troposphere at a global scale in the extra-tropics. CO analyses reduce the spread of the ExTL and O_3 analyses lower the location of the ExTL closer to the thermal tropopause. A combination of these two analyses shows significant better results than each analyses separately: the ExTL location matches the thermal tropopause location at middle and polar latitudes and its spread is in the range of what is observed by in situ and satellite measurements studies. In the Northern Hemisphere Pan et al. (2004) deduced from aircraft observations that the ExTL thickness is 2–3 km at middle latitudes with enhanced values in the vicinity of the subtropical jet. In Table 2, the O_3 analyses vs. CO analyses distribution shows a strandard deviation (2σ) of $\sim$2.8 km between 50° N and 90° N and of $\sim$3.4 km between 20° N and 50° N. Hegglin et al. (2009) found in satellite measurements an ExTL depth in extra-tropical latitudes between 1.5 km and 4 km which match our results of 2 km to 4 km.

ACPD
12, 22023–22057, 2012

5 Discussions and conclusions

In the present study, we use the statistical diagnostics defined by Pan et al. (2004, 2007) to provide a quantitative description of the impact of MLS O_3 and MOPITT CO analyses produced by data assimilation on the ExTL. Firstly, we focus on a STE case study documented and validated by El Amraoui et al. (2010). O_3-CO relationships are used to characterize the height and depth of the ExTL. Two different O_3 fields are provided, a MOCAGE free model run and MLS analyses, and two different CO fields are provided, a MOCAGE free model run and MOPITT analyses. Then four O_3-CO relationships are studied.

The free model run O_3-CO relationship shows a 3-km wide ExTL distribution which is centered 0.5 km above the 360-K isentrope (1.5 km above the thermal tropopause). This distribution shows the typical behavior of the models representing the atmospheric composition, namely an overestimation of the ExTL depth and of its location in height, above the thermal tropopause. MLS O_3 analyses extend the spread of the distribution toward tropospheric altitudes due to an increase of O_3 values in the UTLS. This increases the depth of the ExTL by about 1 km and lowers the mean location, by 1 km, closer to the thermal tropopause. The ExTL distribution has its maximum at the thermal tropopause showing the capability of MLS O_3 analyses to represent STE exchange. MOPITT CO analyses have the capability to sharpen the CO gradient in the UTLS. This reduces the spread of the ExTL on its stratospheric side by about 0.4 km showing a mean location on the 360-K isentrope. Due to the low sensitivity to CO tropospheric variations of the diagnostics used in the present study, MOPITT CO analyses do not show a signature of STE in the ExTL distributions. In combining the information provided by MLS O_3 analyses and MOPITT CO analyses, the ExTL distribution has a more realistic shape and location. The ExTL mean location is centered on the thermal tropopause and the spread of the ExTL is not increased compared to the free model run. It has been shown that models simulate an ExTL deeper than observed in aircraft measurements, and shifted above the thermal tropopause (Hegglin et al.,

ACPD
12, 22023–22057, 2012

2010). This is due to the limited vertical and horizontal resolutions of the models, as well as the lack of representativeness in the aircraft observations. However, data assimilation of CO and O_3 satellite measurements helps to improve the representation of the ExTL and overcomes the limitation due to the relatively low model resolution.

We also extend the diagnostics at global extra-tropical latitudes for the August 2007 time period. MLS O_3 analyses show a spread of the ExTL distribution toward the surface which lowers the mean location of the ExTL, and puts it closer to the thermal tropopause. MOPITT CO analyses reduce the spread of the ExTL on its stratospheric side which also lowers the ExTL mean location closer to the thermal tropopause. When MLS O_3 analyses and MOPITT CO analyses are used together, a synergistic effect is observed. The ExTL location poleward of 50° N and 50° S matches the thermal tropopause and the depth of the ExTL is reduced compared to the free model run O_3-CO diagnostics. As shown in the case study, the STE is characterized by the tropospheric extent of the ExTL. In the global diagnostics, MLS O_3 analyses increase the tropospheric extent of the ExTL distribution below the 2-PVU level showing stratospheric O_3 intrusions into the troposphere.

It is important to note that the ExTL in the extra-tropical southern latitudes (winter) is shallower than in the extra-tropical Northern Hemisphere (summer). This suggests that mixing processes in the UTLS are more active in the Northern Hemisphere than in the Southern Hemisphere. Further investigation is needed, for example using O_3 and CO fields analyses over longer time scales (e.g. more than one year) to diagnose the seasonal behavior of the ExTL.

Acknowledgements. We thank the Jet Propulsion Laboratory MLS science team for retrieving and providing the O_3 MLS data. We thank the National Center for Atmospheric Research MOPITT science team and NASA for producing and archiving the MOPITT CO product. This work was funded by the Centre National de Recherches Scientifiques (CNRS) and the Centre National de Recherches Météorologiques (CNRM) of Météo-France. VHP, JLA, LEA and WL are supported by the RTRA/STAE (POGEQA project). JLA thanks also the Région Midi Pyrénées (INFOAIR project).

ACPD
12, 22023–22057, 2012

The publication of this article is financed by CNRS-INSU.

References

Barré, J., Peuch, V.-H., Attié, J.-L., El Amraoui, L., Lahoz, W. A., Josse, B., Claeyman, M., and Nédélec, P.: Stratosphere-troposphere ozone exchange from high resolution MLS ozone analyses, Atmos. Chem. Phys., 12, 6129–6144, doi:10.5194/acp-12-6129-2012, 2012. 22026, 22027, 22034

Bechtold, P., Bazile, E., Guichard, F., Mascart, P., and Richard, E.: A mass-flux convection scheme for regional and global models, Q. J. Roy. Meteor. Soc., 96, 869–886, 2001. 22027

Bencherif, H., Amraoui, L. E., Sernane, N., Massart, S., Charyulu, D. V., Hauchecorne, A., and Peuch, V.-H.: Examination of the 2002 major warming in the Southern Hemisphere using ground-based and Odin/SMR assimilated data: stratospheric ozone distributions and tropic/mid-latitude exchange, Can. J. Phys., 85, 1287–1300, 2007. 22028

Buis, S., Piacentini, A., and Déclat, D.: PALM: a computational framework for assembling high-performance computing applications, Concurr. Comp.-Pract. E., 18, 231–245, doi:10.1002/cpe.914, 2006. 22027

Courtier, P., Freydier, C., Geleyn, J. F., Rabier, F., and Rochas, M.: The ARPEGE project at Météo France, in: Atmospheric Models, vol. 2, Workshop on Numerical Methods, 9–13 September, Reading, UK, 193–231, 1991. 22027

Drummond, J. R. and Mand, G. S.: Evaluation of operational radiances for the Measurement of Pollution in the Troposphere (MOPITT) instrument CO thermal-band channels, J. Geophys. Res., 109, D03308, doi:10.1029/2003JD003970, 1996. 22028

Dufour, A., Amodei, M., Ancellet, G., and Peuch, V.-H.: Observed and modelled "chemical weather" during ESCOMPTE, Atmos. Res., 74, 161–189, doi:10.1016/j.atmosres.2004.04.013, 2005. 22027

El Amraoui, L., Peuch, V.-H., Ricaud, P., Massart, S., Semane, N., Teyssèdre, H., Cariolle, D., and Karcher, F.: Ozone loss in the 2002–2003 Arctic vortex deduced from the assimilation of Odin/SMR O_3 and N_2O measurements: N_2O as a dynamical tracer, Q. J. Roy. Meteor. Soc., 134, 217–228, doi:10.1002/qj.191, 2008a. 22027, 22028

El Amraoui, L., Semane, N., Peuch, V.-H., and Santee, M. L.: Investigation of dynamical processes in the polar stratospheric vortex during the unusually cold winter 2004/2005, Geophys. Res. Lett., 35, L03803, doi:10.1029/2007GL031251, 2008b. 22028

El Amraoui, L., Attié, J.-L., Semane, N., Claeyman, M., Peuch, V.-H., Warner, J., Ricaud, P., Cammas, J.-P., Piacentini, A., Josse, B., Cariolle, D., Massart, S., and Bencherif, H.: Mid-latitude stratosphere – troposphere exchange as diagnosed by MLS O_3 and MOPITT CO assimilated fields, Atmos. Chem. Phys., 10, 2175–2194, doi:10.5194/acp-10-2175-2010, 2010. 22026, 22028, 22029, 22041

Fischer, H., Wienhold, F. G., Hoor, P., Bujok, O., Schiller, C., Siegmund, P., Ambaum, M., Scheeren, H. A., and Lelieveld, J.: Tracer correlations in the northern high latitude lowermost stratosphere: influence of cross-tropopause mass exchange, Geophys. Res. Lett., 27, 97–100, doi:10.1029/1999GL010879, 2000. 22025, 22031

Fisher, M. and Andersson, E.: Developments in 4D-Var and Kalman filtering, in: Technical Memorandum Research Department, vol. 347, ECMWF, Reading, UK, 2001. 22027

Geer, A. J., Lahoz, W. A., Bekki, S., Bormann, N., Errera, Q., Eskes, H. J., Fonteyn, D., Jackson, D. R., Juckes, M. N., Massart, S., Peuch, V.-H., Rharmili, S., and Segers, A.: The ASSET intercomparison of ozone analyses: method and first results, Atmos. Chem. Phys., 6, 5445–5474, doi:10.5194/acp-6-5445-2006, 2006. 22028

Gettelman, A., Hoor, P., Pan, L. L., Randel, W. J., Hegglin, M. I., and Birner, T.: The extratropical upper troposphere and lower stratosphere, Rev. Geophys., 49, RG3003, doi:10.1029/2011RG000355, 2011. 22038

Hegglin, M. I., Boone, C. D., Manney, G. L., and Walker, K. A.: A global view of the extratropical tropopause transition layer from Atmospheric Chemistry Experiment Fourier Transform Spectrometer O-3, H_2O, and CO, J. Geophys. Res., 114, D00B11, doi:10.1029/2008JD009984, 2009. 22025, 22040

Hegglin, M. I., Gettelman, A., Hoor, P., Krichevsky, R., Manney, G. L., Pan, L. L., Son, S. W., Stiller, G., Tilmes, S., Walker, K. A., Eyring, V., Shepherd, T. G., Waugh, D., Akiyoshi, H., Anel, J. A., Austin, J., Baumgaertner, A., Bekki, S., Braesicke, P., Bruehl, C., Butchart, N., Chipperfield, M., Dameris, M., Dhomse, S., Frith, S., Garny, H., Hardiman, S. C., Joeckel, P.,

ACPD
12, 22023–22057, 2012

Kinnison, D. E., Lamarque, J. F., Mancini, E., Michou, M., Morgenstern, O., Nakamura, T., Olivie, D., Pawson, S., Pitari, G., Plummer, D. A., Pyle, J. A., Rozanov, E., Scinocca, J. F., Shibata, K., Smale, D., Teyssedre, H., Tian, W., and Yamashita, Y.: Multimodel assessment of the upper troposphere and lower stratosphere: extratropics, J. Geophys. Res., 115, D00M09, doi:10.1029/2010JD013884, 2010. 22025, 22035, 22036, 22041

Holton, J. R., Haynes, P. H., McIntyre, M. E., Douglass, A. R., Rood, R. B., and Pfister, L.: Stratosphere-troposphere exchange, Rev. Geophys., 4, 403–439, 1995. 22025

Homeyer, C. R., Bowman, K. P., and Pan, L. L.: Extratropical tropopause transition layer characteristics from high-resolution sounding data, J. Geophys. Res., 115, D13108, doi:10.1029/2009JD013664, 2010. 22033

Hoor, P., Fischer, H., Lange, L., Lelieveld, J., and Brunner, D.: Seasonal variations of a mixing layer in the lowermost stratosphere as identified by the CO-O-3 correlation from in situ measurements, J. Geophys. Res., 107, 4044, doi:10.1029/2000JD000289, 2002. 22025, 22031, 22037

Hoor, P., Gurk, C., Brunner, D., Hegglin, M. I., Wernli, H., and Fischer, H.: Seasonality and extent of extratropical TST derived from in-situ CO measurements during SPURT, Atmos. Chem. Phys., 4, 1427–1442, doi:10.5194/acp-4-1427-2004, 2004. 22031

Josse, B., Simon, P., and Peuch, V.-H.: Radon global simulation with the multiscale chemistry transport model MOCAGE, Tellus, 56, 339–356, 2004. 22027

Kalnay, E.: Atmospheric Modeling, Data Assimilation, and Predictability, University Press, Cambridge, 2003. 22026

Lahoz, W. A., Errera, Q., Swinbank, R., and Fonteyn, D.: Data assimilation of stratospheric constituents: a review, Atmos. Chem. Phys., 7, 5745–5773, doi:10.5194/acp-7-5745-2007, 2007. 22028

Lefèvre, F., Brasseur, G. P., Folkins, I., Smith, A. K., and Simon, P.: Chemistry of the 1991–1992 stratospheric winter: three dimensional model simulations, J. Geophys. Res., 99, 8183–8195, 1994. 22027

Louis, J.-F.: Parametric model of vertical eddy fluxes in the atmosphere, Bound.-Lay. Meteorol., 17, 187–202, 1979. 22027

Massart, S., Cariolle, D., and Peuch, V.-H.: Towards an improvement of the atmospheric ozone distribution and variability by assimilation of satellite data, C.R. Geosci., 337, 1305–1310, doi:10.1016/j.crte.2005.08.001, 2005. 22027

ACPD
12, 22023–22057, 2012

Massart, S., Piacentini, A., Cariolle, D., El Amraoui, L., and Semane, N.: Assessment of the quality of the ozone measurements from the Odin/SMR instrument using data assimilation, Can. J. Phys., 85, 1209–1223, 2007. 22028

Pan, L. L., Randel, W. J., Gary, B. L., Mahoney, M. J., and Hintsa, E. J.: Definitions and sharpness of the extratropical tropopause: a trace gas perspective, J. Geophys. Res., 109, D23103, doi:10.1029/2004JD004982, 2004. 22025, 22031, 22033, 22035, 22036, 22038, 22040, 22041

Pan, L. L., Wei, J. C., Kinnison, D. E., Garcia, R. R., Wuebbles, D. J., and Brasseur, G. P.: A set of diagnostics for evaluating chemistry-climate models in the extratropical tropopause region, J. Geophys. Res., 112, D09316, doi:0.1029/2006JD007792, 2007. 22025, 22026, 22029, 22030, 22031, 22032, 22033, 22035, 22041

Pan, L. L., Randel, W. J., Gille, J. C., Hall, W. D., Nardi, B., Massie, S., Yudin, V., Khosravi, R., Konopka, P., and Tarasick, D.: Tropospheric intrusions associated with the secondary tropopause, J. Geophys. Res., 114, D10302, doi:10.1029/2008JD011374, 2009. 22033

Peuch, V.-H., Amodei, M., Barthet, T., Cathala, M.-L., Michou, M., and Simon, P.: MOCAGE, Modéle de Chimie Atmosphérique à Grande Echelle, in: Proceedings of Météo France: Workshop on atmospheric modelling, December, Toulouse, France, 33–36, 1999. 22027

Ricaud, P., Barret, B., Attié, J.-L., Motte, E., Le Flochmoën, E., Teyssèdre, H., Peuch, V.-H., Livesey, N., Lambert, A., and Pommereau, J.-P.: Impact of land convection on troposphere-stratosphere exchange in the tropics, Atmos. Chem. Phys., 7, 5639–5657, doi:10.5194/acp-7-5639-2007, 2007. 22027

Semane, N., Peuch, V.-H., Amraoui, L. E., Bencherif, H., Massart, S., Cariolle, D., Attié, J.-L., and Abidab, R.: An observed and analysed stratospheric ozone intrusion over the high Canadian Arctic UTLS region during the summer of 2003, Q. J. Roy. Meteor. Soc., 133, 171–178, doi:10.1002/qj.141, 2007. 22026, 22028

Stockwell, W. R., Kirchner, F., Khun, M., and Seefeld, S.: A new mechanism for regional atmospheric chemistry modelling, J. Geophys. Res., 102, 25847–25879, 1997. 22027

Vogel, B., Pan, L. L., Konopka, P., Guenther, G., Mueller, R., Hall, W., Campos, T., Pollack, I., Weinheimer, A., Wei, J., Atlas, E. L., and Bowman, K. P.: Transport pathways and signatures of mixing in the extratropical tropopause region derived from Lagrangian model simulations, J. Geophys. Res., 116, D05306, doi:10.1029/2010JD014876, 2011. 22039

Waters, J. W., Froidevaux, L., Harwood, R. S., Jarnot, R. F., Pickett, H. M., Read, W. G., Siegel, P. H., Cofield, R. E., Filipiak, M. J., Flower, D. A., Holden, J. R., Lau, G. K. K.,

ACPD
12, 22023–22057, 2012

Livesey, N. J., Manney, G. L., Pumphrey, H. C., Santee, M. L., Wu, D. L., Cuddy, D. T., Lay, R. R., Loo, M. S., Perun, V. S., Schwartz, M. J., Stek, P. C., Thurstans, R. P., Boyles, M. A., Chandra, K. M., Chavez, M. C., Chen, G. S., Chudasama, B. V., Dodge, R., Fuller, R. A., Girard, M. A., Jiang, J. H., Jiang, Y. B., Knosp, B. W., LaBelle, R. C., Lam, J. C., Lee, K. A., Miller, D., Oswald, J. E., Patel, N. C., Pukala, D. M., Quintero, O., Scaff, D. M., Snyder, W. V., Tope, M. C., Wagner, P. A., and Walch, M. J.: The Earth Observing System Microwave Limb Sounder (EOS MLS) on the Aura satellite, IEEE T. Geosci. Remote, 44, 1075–7092, 2006. 22028

World Meteorological Organization: Definition of the Tropopause, No. 6, WMO Bull. , Geneva, Switzerland, 1957. 22033

World Meteorological Organization: Atmospheric Ozone: 1985, Global Ozone Research and Monitoring Project Report no. 16, WMO Bull. , Geneva, Switzerland, 1986. 22025

Zahn, A., Brenninkmeijer, C. A. M., Maiss, M., Scharffe, D. H., Crutzen, P. J., Hermann, M., Heintzenberg, J., Wiedensohler, A., Gusten, H., Heinrich, G., Fischer, H., Cuijpers, J. W. M., and van Velthoven, P. F. J.: Identification of extratropical two-way troposphere-stratosphere mixing based on CARIBIC measurements of O-3, CO, and ultrafine particles, J. Geophys. Res., 105, 1527–1535, doi:10.1029/1999JD900759, 2000. 22031

ACPD
12, 22023–22057, 2012

Table 1. Fitting coefficients for the ExTL region of O_3-CO correlations, assuming a quadratic form $y = a_2x^2 + a_1x + a_0$. CO and O_3 values are defined by x and y, respectively.

	a_2	a_1	a_0
model O_3 vs. model CO	9.73×10^{-2}	-1.78×10^{1}	9.11×10^{2}
O_3 analyses vs. model CO	-2.99×10^{-1}	3.07×10^{1}	-3.17×10^{2}
model O_3 vs. CO analyses	5.31×10^{-2}	-9.75	5.77×10^{2}
O_3 analyses vs. CO analyses	-8.84×10^{-2}	7.39	2.80×10^{2}

ACPD
12, 22023–22057, 2012

Table 2. Heights of the mean, median and standard deviation of the ExTL distribution in relative altitude space (km) for the different experiments.

	Mean	Median	Standard deviation
model O_3 vs. model CO	0.58	0.54	1.42
O_3 analyses vs. model CO	−0.39	−0.44	2.01
model O_3 vs. CO analyses	0.008	0.016	1.12
O_3 analyses vs. CO analyses	−0.85	−0.83	1.43

ACPD
12, 22023–22057, 2012

Table 3. Heights of the mean, median and standard deviation of the ExTL distribution in relative altitude space (km) for the different experiments and for the different regions over the globe.

		90° S–50° S	50° S–20° S	20° N–50° N	50° N–90° N
model O_3	Mean	−2.18	−0.40	1.18	0.12
vs. model CO	Median	−2.23	−0.59	0.92	−0.10
	Standard Deviation	0.80	1.57	2.20	1.63
O_3 analyses	Mean	−2.39	−0.76	0.76	−0.62
vs. model CO	Median	−2.46	−0.96	0.41	−0.90
	Standard Deviation	0.93	1.73	2.31	1.92
model O_3	Mean	−2.04	−0.77	0.24	−0.44
vs. CO analyses	Median	−2.08	−0.90	0.11	−0.49
	Standard Deviation	0.64	1.32	1.67	1.05
O_3 analyses	Mean	−2.33	−1.12	−0.12	−1.25
vs. CO analyses	Median	−2.40	−1.27	−0.31	−1.40
	Standard Deviation	0.80	1.45	1.69	1.41

ACPD
12, 22023–22057, 2012

J. Barre et al.

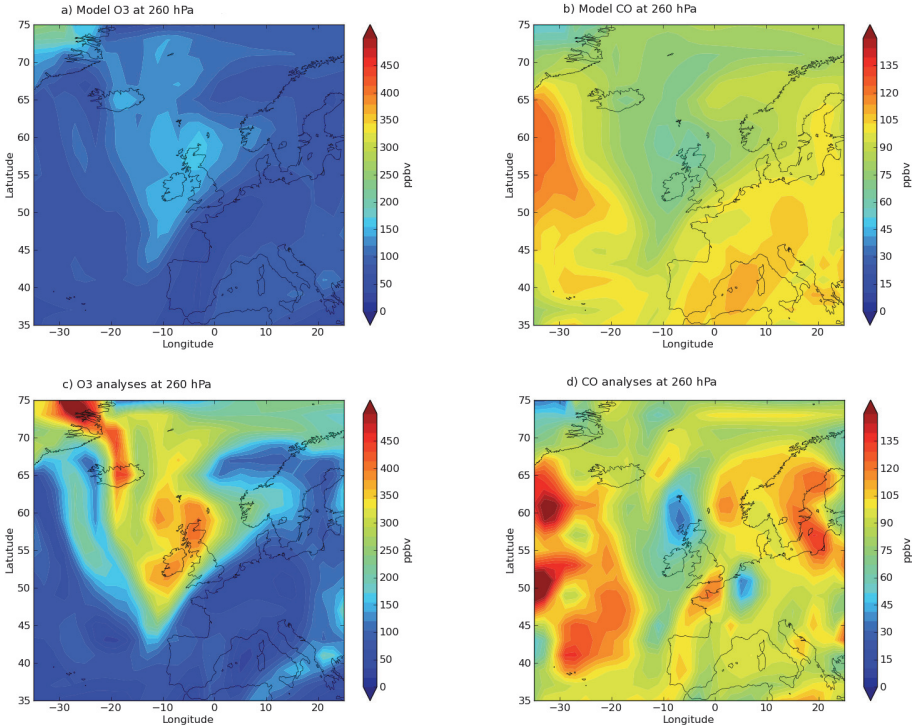

Fig. 1. Longitude-latitude maps at 260 hPa of model O_3 **(a)**, model CO **(b)**, O_3 analyses **(c)** and CO analyses **(d)** for 15 August 2007 at 12:00 UT

ACPD
12, 22023–22057, 2012

J. Barre et al.

Diagnosing the ExTL

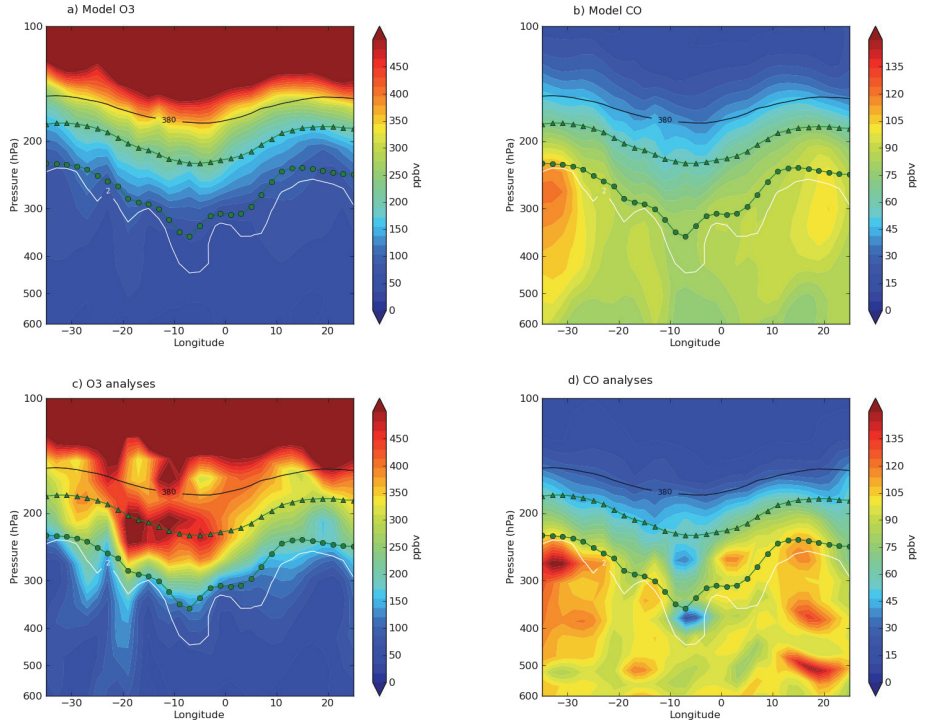

Fig. 2. Zonal cross sections at 59° N between 40° W and 40° E longitude and between 600 and 100 hPa in the vertical for model O_3 **(a)**, model CO **(b)**, O_3 analyses **(c)** and CO analyses **(d)**. The white line corresponds to the 2 potential vorticity units contour. The black line and green triangles correspond to the 380-K and 360-K isentropic contours, respectively. The green circle corresponds to the thermal tropopause. Panels are for 15 August 2007 at 12:00 UT.

ACPD
12, 22023–22057, 2012

J. Barre et al.

Diagnosing the ExTL

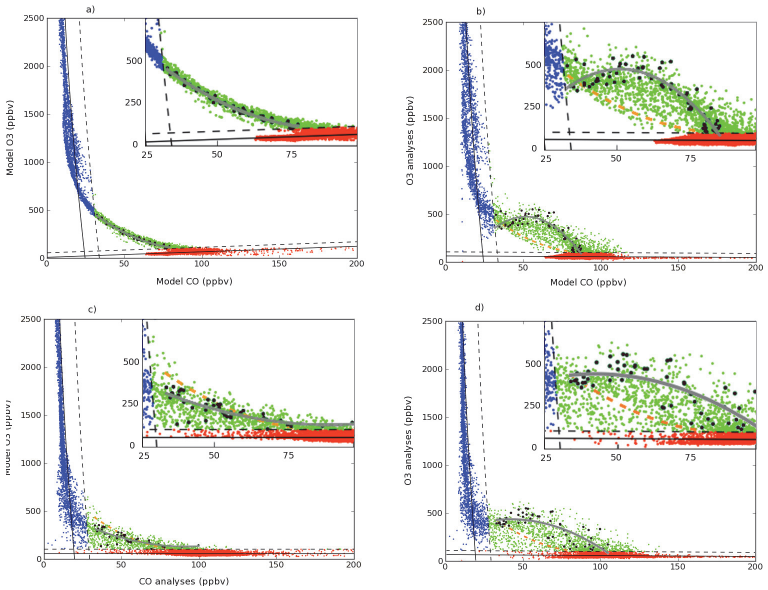

Fig. 3. Comparisons of the O_3-CO relationships between model O_3 vs. model CO **(a)**, O_3 analyses vs. model CO **(b)**, model O_3 vs. CO analyses **(c)** and O_3 analyses vs. CO analyses **(d)** in the area between 30° W–10° E, 40° N–65° N on 15 August 2007 at 12:00 UT. In all cases, red and blue dots are identified as tropospheric and stratospheric model grid points, respectively. Black solid lines indicate fits to tropospheric and stratospheric values and the dashed lines are the $+3\sigma$ values (where σ is the standard deviation of the selected data) from those fits. The green dots are identified as the transition between stratospheric and tropospheric air. The transitional points between 20° W and 0° W on the 59° N vertical plane are in black and are fitted by the gray line. The model O_3 vs. model CO fit is over-plotted on **(b–d)** in dashed orange (see text for details). Within each plot box a zoom of the transition region is provided (top-right) on each panel.

ACPD
12, 22023–22057, 2012

J. Barre et al.

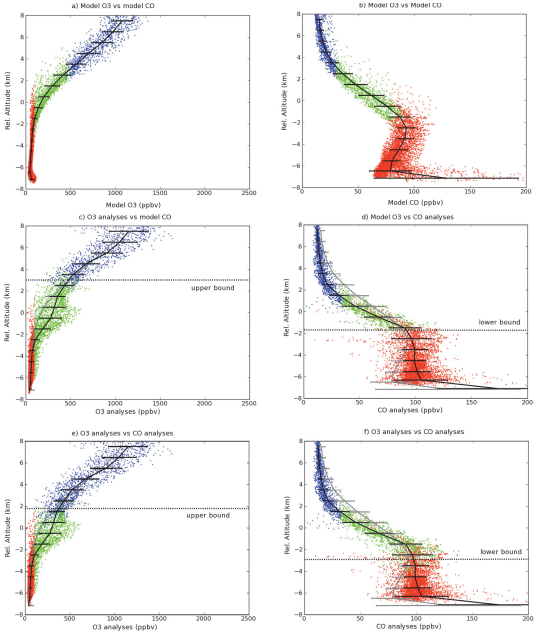

Fig. 4. O_3 and CO profiles in the region between 30° W–10° E, 40° N–65° N on 15 August 2007 at 12:00 UT. O_3 profiles (ppbv) in altitude coordinates (km) relative to the 360-K level are provided for model O_3 vs. model CO **(a)**, O_3 analyses vs. model CO **(c)** and O_3 analyses vs. CO analyses **(e)**. CO profiles (ppbv) in relative altitude coordinates (km) are provided for model O_3 vs. model CO **(b)**, model O_3 vs. CO analyses **(d)** and O_3 analyses vs. CO analyses **(f)**. Following selection criteria, red and blue dots are identified as of tropospheric and stratospheric origin, respectively. The green dots are identified as the transitional layer between the stratosphere and the troposphere (see text for details). Black lines represent the mean profile every kilometer and horizontal error bars show the 1σ standard deviation. Over-plotted gray lines and gray error bars **(c–f)** are the free model run mean and standard deviation values for O_3 and CO, respectively.

ACPD
12, 22023–22057, 2012

J. Barre et al.

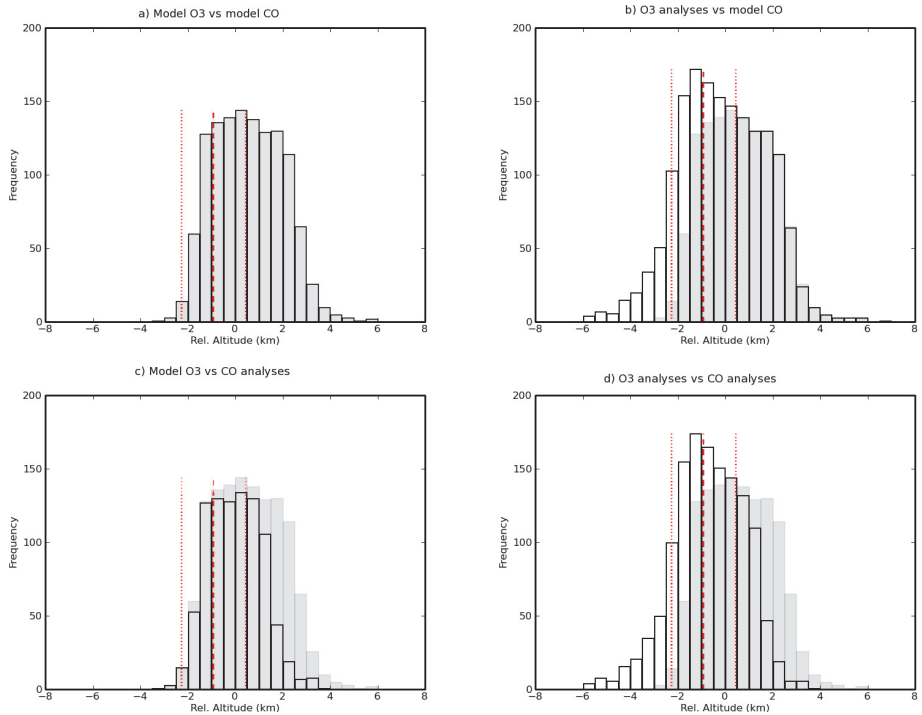

Fig. 5. Histograms showing the distributions of the ExTL in relative altitude space in the region between 30° W–10° E, 40° N–65° N on 15 August 2007 at 12:00 UT. Model O_3 vs. model CO **(a)**, O_3 analyses vs. model CO **(b)**, model O_3 vs. CO analyses **(c)** and O_3 analyses vs. CO analyses **(d)** are displayed in black and model O_3 vs. model CO distribution is over-plotted in gray on the plots. Red dashed and dotted vertical lines line show the mean and the standard deviation of the location of the thermal tropopause, respectively. The histograms display the absolute frequencies.

ACPD
12, 22023–22057, 2012

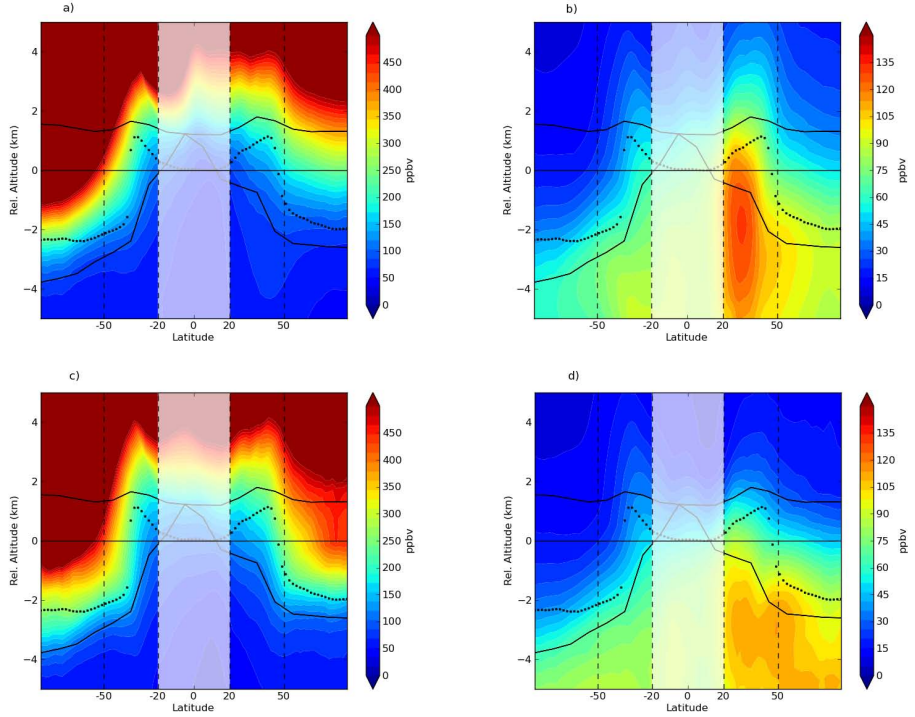

Fig. 6. Zonal averages for the month of August 2007 in relatives altitudes (km) of model O_3 **(a)**, model CO **(b)**, O_3 analyses **(c)** and CO analyses **(d)**. Dashed black vertical lines mark the regions of interest. The lowermost stratosphere bounds are represented by the 2-PVU contour in absolute value (lower black line), and the 380-K isentrope (upper black line). Black dots are the thermal tropopause relative altitudes. Tropical latitudes are not shown.

ACPD
12, 22023–22057, 2012

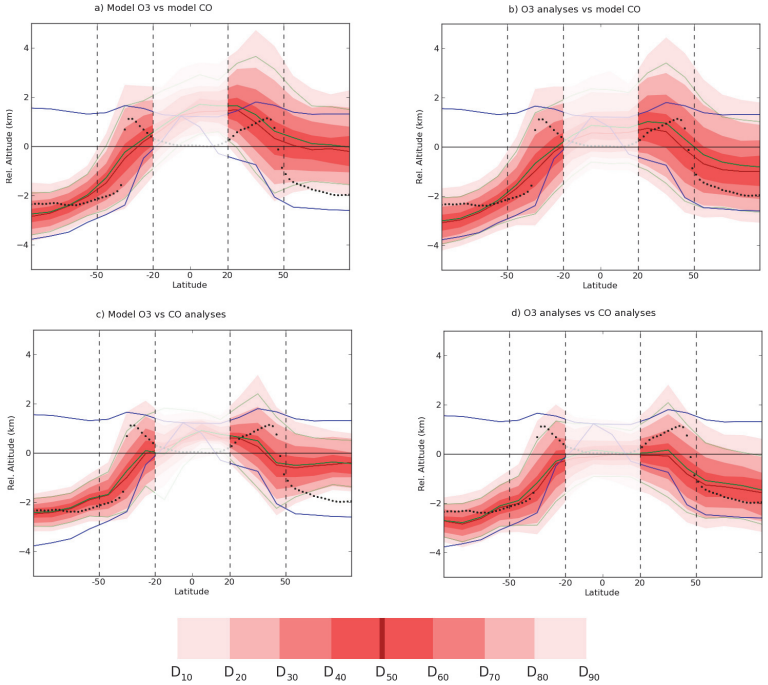

Fig. 7. Latitudinal height variations in altitude coordinates (km) relative to the 360-K level of the ExTL distribution for model O_3 vs. model CO **(a)**, O_3 analyses vs. model CO **(b)**, model O_3 vs. CO analyses **(c)** and O_3 analyses vs. CO analyses **(d)** in August 2007. Red filled contours provide the decile altitudes of the distribution. Red and green lines are the median and mean altitudes, respectively. Blue lines show the lowermost stratosphere bounds: the lower line provides the 2-PVU contour in absolute value, the upper line provides the 380-K isentropic contour. Black dots show the location of the thermal tropopause. Tropical latitudes are not shown.

ACPD
12, 22023–22057, 2012

J. Barre et al.